Stretching biological cells with light

2002 J. Phys.: Condens. Matter 14 4843

(http://iopscience.iop.org/0953-8984/14/19/311)

INSTITUTE OF PHYSICS PUBLISHING JOURNAL OF PHYSICS: CONDENSED MATTER

J. Phys.: Condens. Matter **14** (2002) 4843–4856 PII: S0953-8984(02)29158-4

Stretching biological cells with light

Jochen Guck[1], **Revathi Ananthakrishnan**[1], **C Casey Cunningham**[2] **and Josef Käs**[1,3,4,5]

[1] Address for Correspondence: Center for Nonlinear Dynamics, Department of Physics, University of Texas at Austin, Austin, TX 78712, USA
[2] Collins Bldg, Baylor University Medical Center, Dallas, TX 75246, USA
[3] Institute for Molecular and Cellular Biology, University of Texas at Austin, Austin, TX 78712, USA
[4] Texas Materials Institute, University of Texas at Austin, Austin, TX 78712, USA

E-mail: kas@chaos.ph.utexas.edu

Received 26 September 2001
Published 2 May 2002
Online at stacks.iop.org/JPhysCM/14/4843

Abstract

The radiation pressure of two counter-propagating laser beams traps and stretches individual biological cells. Using non-focused laser beams, cells stay viable when irradiated with up to 1.4 W of 780 nm Ti–sapphire laser light for several minutes. Fluorescence microscopy has demonstrated that the essential features of the cytoskeleton, excluding stress fibres, are maintained for stretched cells in suspension. The optical stretcher provides accurate measurements of whole cell elasticity and thus can distinguish between different cells by their cytoskeletal characteristics. A model has been derived for the forces on the surface of a spherical cell that explains the observed deformations. The peak stresses on the surface of cells are 1–150 Pa for light powers of 0.2–1.4 W and depending on the refractive index of the cell trapped. Precursors of rat nerve cells exhibit a homogeneous Young's modulus $\boldsymbol{E}$ of 500 ± 25 Pa, whereas for osmotically inflated, spherical red blood cells (RBCs) the homogeneous Young's modulus is $\boldsymbol{E} = 11.0 \pm 0.5$ Pa. Thus, PC12 cells are about 40–50 times more elastic than RBCs.

(Some figures in this article are in colour only in the electronic version)

1. Introduction

The momentum of photons of a certain wavelength is in general very small compared with the absolute momenta encountered in our immediate environment. Consequently, the momentum transfer of photons can be neglected in almost all cases. In the microscopic world, however, this transfer of momentum is important and can be used to manipulate particles ranging in

[5] Center for Nano- and Molecular Science and Technology, University of Texas at Austin, Austin, TX 78712, USA.

size from atoms to micron-sized beads or biological cells [1–4]. The laser cooling and trapping of atoms is an actual example at the lower end of this range [5–7]. An example on the other end of the dimensional range is the manipulation of biological objects such as cells and cell organelles. The most common laser tools for the manipulation of biological materials are optical tweezers [8–13]. For instance, they are used for the trapping of cells and bacteria [14, 15], for the measuring of the forces exerted by molecular motors such as myosin or kinesin [16–20], or the swimming forces of sperm [21, 22], and for the study of the mechanical properties of single DNA strands fully expanded by means of beads attached to their ends [5, 23]. A similar trap, the optical spanner, exploits the conservation of angular momentum to also rotate particles. However, these tools are only capable of facilitating translation and rotation of objects. Also, their geometries with focused laser beams lead to an early onset of radiation damage of biological matter and limit the applicable light power, i.e. force range. Recently, it has been reported for the first time that the forces arising from the interaction of light with matter can be used to intentionally deform cells in a controlled and nondestructive manner [25, 26]. With the optical stretcher it is possible to measure the elasticity of deformable objects, such as cells, with diameters ranging from 5 to 50 μm.

With this novel tool it is possible to shed new light on the amazing mechanical strength of cells. Eukaryotic cells owe their stability to a three-dimensional network of protein filaments, known as the cytoskeleton. The principal components of the cytoskeleton are microtubules, intermediate filaments, and actin filaments. In non-mitotic cells, the microtubules radiate radially outward from the microtubule-organizing centre, which lies just outside the cell nucleus, to the cell's periphery. Intermediate filaments are unique to multicellular organisms and different kinds of differentiated cell usually contain specific types of intermediate filament. For example, vimentin is expressed in mesenchymal cells (e.g. fibroblasts). Vimentin fibres often terminate at the nuclear membrane and at desmosomes or adhesion plaques on the plasma membrane. They are often co-localized with microtubules, suggesting a close association between the two filament networks. The actin cytoskeleton can be roughly divided into two superimposing elastic elements: a homogeneous filamentous protein network, the actin cortex, which predominantly underlies the plasma membrane, and stress fibres, which span the entire cell interior and start at focal adhesion plaques of the plasma membrane. The filamentous protein myosin is closely associated with actin. The mechanisms, how these components are able to provide mechanical stability to cells, are only poorly understood, as classical concepts in polymer physics fail to explain this phenomenon [24].

The obvious importance for a cell to withstand deforming stresses has motivated the development of several systems to measure cell elasticities. However, each of these methods has severe limitations. Due to small size ($\approx$10 μm) and mechanical strength ($\approx$10–1000 Pa) of cells, it is difficult to obtain reliable and precise data. Atomic-force microscopy [27], manipulation with micro-needles [28], cell stretching between two plates [29] and cell poking [30] are not able to detect small variations in cell elasticity because their detection devices have a very high spring constant compared with the elastic modulus of the material probed. Micropipette-aspiration experiments [31] can provide inaccurate measurements if the plasma membrane becomes detached from the cytoskeleton. Displacement of surface-attached microspheres [32] depends on the coupling of the plasma membrane to the cytoskeleton. In addition, these techniques only look at the elasticity of the cell over a relatively small area of its surface. Whole cell elasticity can be indirectly investigated by measurements of the compression and shear moduli of densely packed cell pellets [33, 34]. However, these measurements only represent an average value, rather than a true single-cell measurement, and

also depend on non-cytoskeletal forces such as cell–cell adhesion. The optical stretcher is a new tool that circumvents these problems.

2. Theory

The trapping of particles with one or more laser beams is understood relatively well. However, it might not be generally realized that the trapping forces also have the potential to deform particles. For the optical stretcher, a two-beam arrangement as described by Constable *et al* [38] is used to capture a single cell. The light power in both beams is then increased to the point where the radiation pressure begins to detectably deform the cell. One would expect that the cell is squeezed between the two beams since the total scattering force of each beam acts in the direction of the propagation of the light and pushes the cell in the direction of light propagation. Exactly the opposite is true. The cell is axially stretched out [25, 26]. The calculation of these deforming forces starts from the same point as previous discussions of particle trapping [9, 12, 35], but emphasizes a different aspect. The following summary introduces the basic principles and is intended to point out differences between former publications and this study.

For most biological applications, such as here described, ray-optics provides a valid approach for the interaction of light with matter because the size of the objects of interest is much larger than the wavelength of the laser light. The diameter of cells is on the order of tens of microns. Most cell biological experiments are performed in aqueous solution and water is sufficiently transparent only for electromagnetic radiation with wavelengths less than one micron (the Ti–sapphire laser was operated at a wavelength of 780 nm) so that the criterion for the use of ray-optics is fulfilled. The approach in this regime is to decompose an incident light beam into individual rays with an appropriate intensity, momentum and direction. These rays propagate in straight lines in uniform, nondispersive media and can be treated in a geometrical optics picture. When such a ray hits the interface of two different dielectric media with refractive indices n_1 and n_2 under an angle θ, it changes direction according to Snell's law, $n_1 \sin\theta = n_2 \sin r$, where r is the angle of the refracted ray. Some energy of the ray is reflected at the interface. The fractions of the energy T and R in the refracted and the reflected part, respectively, are given by equations (4) and (5). Each ray also carries a certain amount of momentum p proportional to its energy E and the refractive index n of the medium it travels in

$$p = \frac{E \cdot n}{c} \tag{1}$$

where c is the speed of light [37]. This momentum has to be conserved at the interface. When a light ray hits a particle, the momentum of the ray changes in direction and magnitude, and the difference is picked up by the particle which consequently feels a force

$$F = \frac{\Delta p}{\Delta t} = \frac{\Delta E \cdot n}{\Delta t \cdot c} = \frac{P \cdot n}{c} \tag{2}$$

where P is the power contained in the ray. This force can be calculated for a ray with a certain incident angle θ and for all subsequent refracted and reflected rays on a sphere. Summing up over all incident angles yields the total force on the particle's centre of mass. Due to the cylindrical symmetry this force has only a component in the direction of the light propagation which is called scattering force. If the particle is in a laser beam with Gaussian profile, the symmetry is broken when the particle is displaced from the beam axis. It feels a restoring force perpendicular to the axis, which is called gradient force. In the Rayleigh regime (wavelength of the light much larger than the object) particles are treated as point dipoles, which qualitatively experience the same kind of force in a laser beam. For the intermediate case, where the wavelength of the light is comparable to the dimension of the object, the theoretical discussion

of the forces is complex and difficult. However, in experiments also these objects show the same qualitative behaviour. Regardless of the regime, a laser beam with Gaussian profile pulls the particle towards its symmetry axis and pushes the particle in the direction of the beam propagation.

In the trapping scenarios previously described, either non-deformable particles (glass beads, latex beads) were used or the goal was solely to trap, hold, move, and/or rotate these particles. The new idea presented in this paper is to use a two-beam trap to capture a single cell and then to increase the light power to the point where the radiation pressure begins to deform the cell. This stretching is very similar to the situation where a laser beam enters or exits a dielectric liquid and exerts a net outward force and causes the surface to bend. This effect has been predicted by Kats and Kantorovich [39] and has been shown experimentally by Ashkin and Dziedzic [37]. For a cell this effect must be generalized to spherical geometry.

To calculate the deforming force profile a cell is assumed to be a spherical, homogeneous, and lossless dielectric particle with a certain index of refraction n_2 suspended in a fluid with refractive index n_1. The assumption of a spherical particle is in good agreement with the experimental situation. Cells are also rather transparent and hard to see in a through-light microscope, which makes the assumption of a non-absorbing particle plausible. The homogeneity of the particle is a necessary assumption to keep the calculation simple, but is questionable for a cell with all its small, localized structures, for example the nucleus, Golgi apparatus and mitochondria. The relative index of refraction $n = n_2/n_1 > 1$ is on the order of 1.03–1.15 for biological materials in aqueous solutions [9, 10, 25].

For the total force acting on the cell's centre of mass the momentum of the light inside the cell is not relevant, since it is sufficient to compare the momentum of the incident and the transmitted light. The difference is picked up by the particle, which feels a total force acting on its centre. For the calculation of the deforming forces, however, the situation at every surface element of the cell is of interest. The fact that the momentum of light changes when it enters or leaves a medium with different optical properties is essential and must not be neglected. Depending on the incident angle, some light is always reflected backwards and not all energy enters the medium. However, the effect of the increase in momentum due to the higher refractive index inside the cell dominates the decrease that is caused by reflection because cells are almost transparent. This leads to the outward force rather than an inward force. The net change in momentum,

$$\Delta\vec{p} = \vec{p}_1 - \vec{p}_2 - \vec{p}_r \tag{3}$$

where the momentum of the incident ray $p_1 = En_1/c \equiv 1$, the momentum of the reflected ray $p_\mathrm{r} = R(\theta)En_1/c = R(\theta)$ and the momentum of the transmitted ray $p_2 = T(\theta)En_2/c = T(\theta)n_2/n_1 = T(\theta)n$, is balanced by a mechanical force on the medium proportional to Δp (see also figure 1). The transmission and reflection coefficients, $T(\theta)$ and $R(\theta)$, are taken to be

$$T(\theta) = \frac{t_\perp^2(\theta) + t_\parallel^2(\theta)}{2} \tag{4}$$

and

$$R(\theta) = \frac{r_\perp^2(\theta) + r_\parallel^2(\theta)}{2} \tag{5}$$

where $t_\perp$, $t_\parallel$, $r_\perp$ and $r_\parallel$ are the usual Fresnel coefficients for the transmitted and reflected TE and TM field amplitudes, each for parallel and perpendicular orientation with respect to the plane of incidence [36, 41].

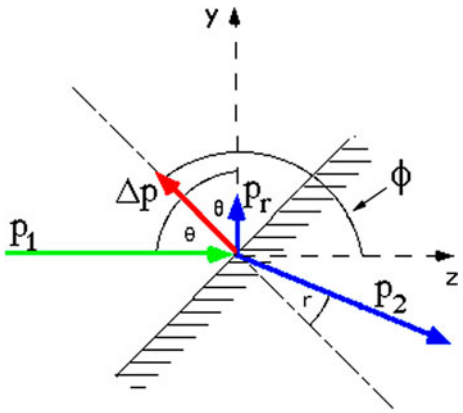

Figure 1. Momentum of light rays at the interface between two media.

The components of the resulting change in momentum in z and y directions, as functions of the incident angle θ, are

$$\begin{aligned}\Delta p_z &= \Delta p \cdot \cos\phi = p_1 \cos(0) - p_2 \cos(2\pi - \theta + r) - p_r \cos(\pi - 2\theta) \\ &= 1 - T(\theta) \cdot n \cdot \cos(\theta - r) + R(\theta) \cdot \cos(2\theta) \end{aligned} \tag{6}$$

and

$$\begin{aligned}\Delta p_y &= \Delta p \cdot \sin\phi = p_1 \sin(0) - p_2 \sin(2\pi - \theta + r) - p_r \sin(\pi - 2\theta) \\ &= T(\theta) \cdot n \cdot \sin(\theta - r) + R(\theta) \cdot \sin(2\theta). \end{aligned} \tag{7}$$

The magnitude of Δp is then given by

$$\Delta p = \sqrt{\Delta p_z^2 + \Delta p_y^2} \tag{8}$$

and its direction is

$$\phi = \arctan\left(\frac{\Delta p_y}{\Delta p_z}\right). \tag{9}$$

These quantities can be numerically calculated and plotted for the surface of a sphere. The relative index of refraction can be determined by index matching in phase-contrast microscopy [25] and absorption is neglected as explained above. It should be noted that the sphere acts as a lens. Thus, the rays are collected close to the axis where the beam leaves the sphere. This gives rise to forces that are also pointing away from the surface at the back of the sphere. Figure 2 shows the stress profile on a dielectric sphere due to one laser beam with Gaussian profile. The lens effect causes the forces on the backside to mainly point in the forward ($+z$) direction whereas the forces on the front side have larger components in the perpendicular (y) direction. The net force on the sphere is in the forward direction in agreement with the action of the scattering force as previously discussed. As long as the cell is free to move it will not be deformed, but rather be pushed in the direction of the net force.

Figure 3 shows the situation for two counter-propagating Gaussian laser beams. The forces are normal to the surface and decrease towards the edge of the particle depending on the ratio between sphere radius ρ and beam radius w, ρ/w. The stress in the middle of the beam is calculated to be about 40 Pa for $n = 1.1$ and 500 mW laser power, and depends linearly on this quantity. This is a stable trapping situation, the particle cannot move, and the surface will deform according to the forces acting on the surface. The cytoskeleton in a cell, which

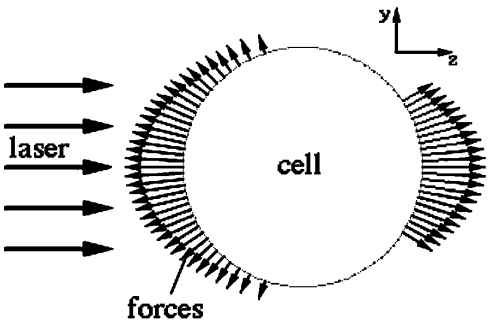

Figure 2. Stress profile on a sphere due to one laser beam.

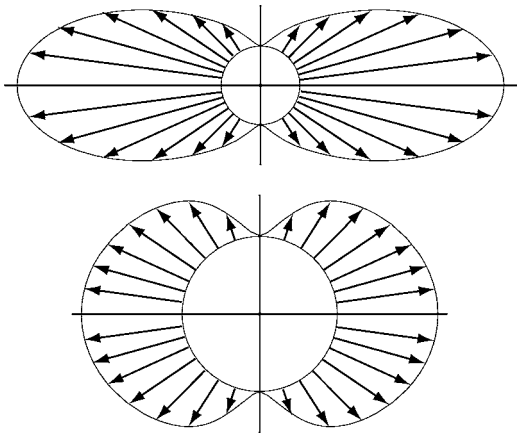

Figure 3. Deforming stresses on a cell trapped between two counter-propagating laser beams. In the upper picture the laser beam has the same radius as the cell ($\rho/w = 1$), whereas in the picture below the laser beam is twice as wide ($\rho/w = 1/2$).

is connected to the plasma membrane, acts as a spring and builds up a restoring tension. The forces on the surface will change corresponding to the deformation until the system reaches equilibrium. The final form of the cell is expected to look like an ellipsoid with the major axis in the direction of the beam axis. In a hand-waving argument, this effect is similar to the case where a dielectric fluid is pulled into the field between two capacitor plates because it is an energetically favourable position. Here the cell is also pulled into the region of higher fields, i.e. the centre of the laser beams.

It is interesting to note that the relative index of refraction, which was assumed to be $n = 1.1$, has a strong influence on the absolute magnitude of the forces. A slight increase in this number to $n = 1.2$, which is a high value for biological materials, has only a small effect on the qualitative shape of the force profile. The lens effect is a little bit stronger than for $n = 1.1$ and leads to an increased collimation of the rays on the backside of the cell. However, the absolute quantities turn out to change more drastically. The peak stress on one side for the two-beam trapping situation is 74 Pa for 500 mW and thus about twice as big as for $n = 1.1$. Thus, it is important to determine the real index of refraction as well as possible.

For an estimate of the homogeneous Young's modulus E of the object, the radial deformation of the cell surface has to be related to the stress that is acting on the surface due to the laser forces. Since the forces are all normal to the surface, the calculation of the

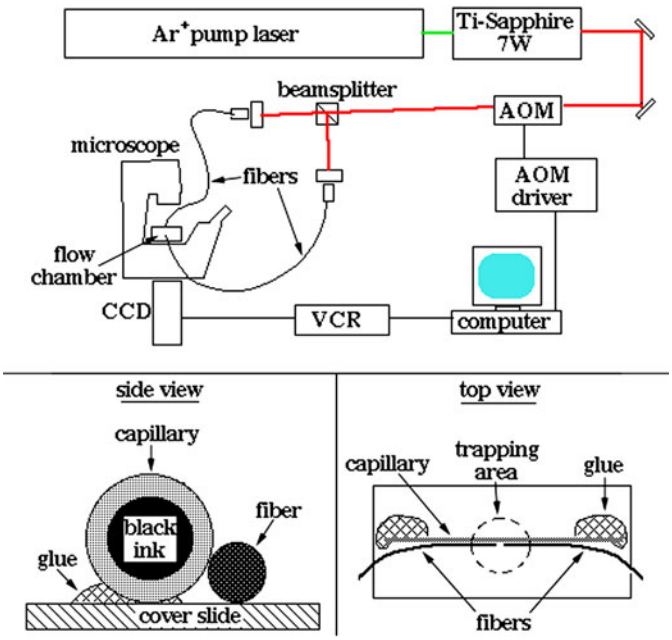

Figure 4. Schematic setup of the optical stretcher (upper panel). Schematic diagram of the alignment of the fibres (lower panel). The cover slide is 25×75 mm^2, the diameter of the capillary is 250–400 μm and the diameter of the fibres is 125 μm.

stress is simply accomplished by using the intensity I rather than the power P of the incident rays in equations (1)–(3). The functional dependence of the radial deformation along the laser axis for a solid sphere with a Young's modulus E subjected to the stress profile in the optical stretcher is given by

$$u_r = \frac{\rho\sigma}{2E}\left(\frac{m-2}{m+1} - \frac{8-14m}{5+7m}\right) \tag{10}$$

where ρ is the radius, σ is the stress and m is the inverse of the Poisson ratio ν [40]. Using this equation and assuming an incompressible material with a Poisson ratio $\nu = 0.5$, the homogeneous Young's modulus of a cell, E, can be found by fitting to the experimental data.

3. Experiments

3.1. Experimental setup

The setup of the experiment (figure 4) is a two-beam fibre trap as in [38]. A tunable, cw Ti–sapphire laser (Spectra Physics Lasers, Inc., 3900S) with up to 7 W of light power is used as light source. The beam is modulated by an acousto-optic modulator (AOM) (IntraAction, AOM-802N), split in two by a non-polarizing beam-splitting cube (Newport Corp.), and then coupled into optical fibres. The fibre couplers were bought from Oz Optics Ltd, the single-mode optical fibres from Newport. With the AOM the light intensity, i.e. the applied stress, can be varied and time-dependent measurements can be performed. The optical fibres do not only simplify the setup of the experiment; they also serve as additional spatial filters and guarantee a good mode quality. Single-mode fibres are used because they display a clean Gaussian profile with an appropriate intensity gradient towards the beam axis. One could imagine using

a multi-mode fibre, which is capable of transmitting much higher light powers at the cost of transmitting higher modes. However, in this application a Gaussian beam profile is required for stable trapping. Another problem with multi-mode fibres is that they have light-guiding cores that are much larger than the cells trapped. Most of the light emanating from a multi-mode fibre would not even hit the cell and could not contribute to the stretching. Thus, the use of multi-mode fibres is not indicated. At present, the highest possible light powers in this setup are up to 1.4 W in each single-mode fibre, which is sufficient to achieve deformations up to 10%.

For the trapping and the stretching of cells the alignment of the fibres is crucial. A glass capillary with a diameter between 250 and 400 μm is glued down on a coverslide and the fibres are pressed against it. Sitting in this crevice formed by the capillary and the slide the fibres are facing each other with appropriate accuracy. This coverslide is mounted on an inverted microscope (Zeiss Axiovert TV100) equipped for phase contrast (Zeiss LD-Achroplan, 40×, 0.60 NA, phase objective) and fluorescence microscopy (Plan-Neofluar, 63×, 1.25 NA, oil objective). Images of the trapping and stretching are obtained with a CCD camera (MTI-Dage CCD72S) and recorded on an SVHS recorder (Panasonic DS550). These images are then evaluated on a PowerComputing computer (PowerTower Pro 225) with NIH-Scion Image software (V 1.60). The pixel size for all used magnifications was calibrated with a 100 lines mm^{-1} grating which allowed for absolute distance measurements.

The stretching of cells is typically on the order of several hundred nanometres. To detect this subtle deformation we have developed an algorithm that enables us to detect deformations with a resolution of ±50 nm [26]. Using this algorithm, the relative deformation of the cell along the laser axis is recorded. Five consecutive pictures before and after the laser power is increased are taken to obtain mean values.

3.2. Sample preparation

As initial test objects red blood cells (RBCs) have been chosen because RBCs are easy to obtain, lack any organelles and can be osmotically swollen to a spherical shape. Thus, RBCs come close to a dielectric sphere without internal structure, as assumed in the model calculations. Another advantage is that RBCs do not have an extensive three-dimensional cytoskeleton but rather a two-dimensional rim right beneath the membrane. Thus, they are much softer than regular cells and should deform more easily. The preparation of the RBCs has been described previously [26]. Their index of refraction was 1.378 ± 0.005 [25].

In contrast to RBCs, eukaryotic cells have a three-dimensional cytoskeleton throughout the whole cell body, which results in a higher mechanical strength. As prototypic eukaryotic cells undifferentiated PC12 rat nerve cells were investigated. These cells are cultured in petri dishes and are usually attached to the surface and clustered together. The culture medium is Dulbecco's modified Eagle's medium (DMEM) with 10% horse serum, 5% FBS (foetal bovine serum) and 1% of an antibiotic–antimycotic solution (penicillin–streptomycin). In order to detach them from the surface, they have to be treated with 0.25% trypsin–EDTA solution (TRED). Trypsin is a protease, which degrades the extracellular matrix and also adhesion receptors. EDTA is a chelating (binding) agent for divalent cations (Ca^{2+}, Mg^{2+}) required for the proper conformation of these receptors. The result of this treatment is that the cells do not cluster together or reattach to the surface for 2–4 h, and assume a nearly spherical shape. Their refractive index was 1.3750 ± 0.0025.

To visualize the actin cytoskeleton, trypsinized PC12 cells are labelled with rhodamine–phalloidin (TRITC). This fluorescence dye stains actin filaments but not single actin monomers, and its fluorescence increases by a factor of three when bound to a filament. This assures that

filaments are predominantly visualized. For the staining, 1 μl of TRITC in dimethylsulfoxide (DMSO) is added to 100 μl cell suspension. By repeated trigeration (sucking in and squirting out of the suspension with a pipette) the membrane is transiently permeabilized and the dye is absorbed by the cell. To reduce the background fluorescence the amount of remaining TRITC in the suspension is reduced by centrifugation and by resuspension of the cells in fresh buffer.

3.3. Viability of cells in the optical stretcher

The viability of the cells under investigation is an important issue since dead cells do not maintain a representative cytoskeleton. It is not obvious that it is possible to use high-intensity laser beams for the deformation of such delicate objects as cells without causing any harm to them. The biggest disadvantage of optical tweezers is that the extreme focusing leads to very high intensities that can endanger the integrity of biological objects. Most cells trapped with optical tweezers do not survive light powers greater than 20–250 mW depending on the specific cell type and the used wavelength [11, 14, 15]. The optical stretcher circumvents this problem. The beams are not focused and the intensities are lower than in optical tweezers by about three orders of magnitude. Thus, higher light powers can be used without the danger of 'opticution'.

Another important consideration is the careful choice of the least damaging wavelength in these experiments. In Ashkin's early experiments, the 530 nm line of an Ar^+-laser was used because it was the most convenient and stable laser source at this time. For the trapping of inanimate matter, such as glass or silica beads, the wavelength is not very important. A short wavelength might be desirable for optical tweezers because the photons have a higher energy and, since the diffraction-limited spot size of a focused beam is on the order of half the wavelength, it allows for higher gradients and better trapping efficiencies. However, these short wavelengths are not appropriate to preserve biological objects such as cells. Therefore, researchers resorted to the 1064 nm of Nd–YAG lasers, and achieved better results [15]. Today, most optical tweezers used for biological applications utilize a Nd–YAG laser, but this is not optimal either. The absorption of chromophores, which is the term for predominantly absorbing components in a cell, is low in the infrared (IR) and increases with decreasing wavelength [4]. The absorption peaks of proteins, for example, lie in the ultraviolet (UV) region. This fact is utilized to measure their concentration in a solution by absorption spectrometry. Nevertheless, the main content of a cell is water ($\approx$70% of the weight [42]), which absorbs increasingly with larger wavelength. At around 800 nm these contrary trends—decreasing protein absorption and increasing water absorption with increasing wavelength—balance each other. Thus thermal heating of the sample should be minimized. For this reason a Ti–sapphire laser at its peak emission of about 780 nm is used for the optical stretcher.

Even though the wavelength used is far away from the absorption bands of proteins, nonlinear optical effects could cause absorption of laser light. Pulsed Ti–sapphire lasers are used in the IR for multi-photon spectroscopy and microscopy to exactly excite these UV absorption bands of proteins. The intensities in the optical stretcher are much smaller than those encountered with pulsed lasers used for multi-photon excitation. Further, the tunability of the Ti–sapphire laser from 600 to 1000 nm allows changing the wavelength, if multi-photon absorption occurs. Consequently, these nonlinear effects can be neglected and should not cause any problems.

Even though care has been taken to avoid possible damaging of cells in the optical stretcher their viability has to be checked on a case-by-case basis. For PC12 cells, the appearance is significantly different when they are not alive. Living cells under a phase-

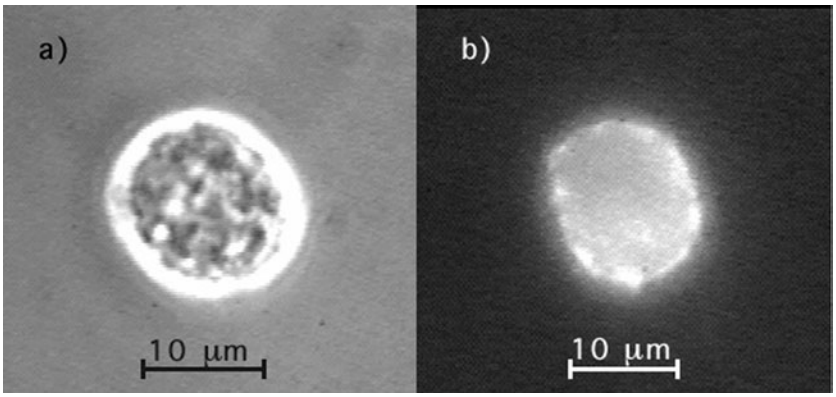

Figure 5. (*a*) Trapped PC12 cell in phase contrast, (*b*) the same cell in fluorescence microscopy. Due to the rhodamine–phalloidin staining the actin cytoskeleton—particularly the cortical rim—is clearly visible.

contrast microscope show a characteristic bright rim around the edge. Dead cells usually have no sharp contour and appear diffuse. After a cell had been trapped and stretched for several minutes, it was always followed sinking down to the cover slide where it was compared with other cells that had not been irradiated. In all cases the cells looked alike. A more careful approach is the use of the vital stain trypan blue. As long as a cell is alive it is able to prevent the dye from entering the cytoplasm. When the cell is dead or does not maintain its normal function, the dye will penetrate the cell membrane and the whole cell appears blue. After adding 5% trypan blue to the cell solution no staining was observed, which indicated that the cells functioned normally. A last, analytical, check was carried out on cells in culture dishes. Four culture dishes were each loaded with $(1.6 \pm 0.2) \times 10^5$ cells. Two of those were irradiated with 500 mW of 780 nm laser light for 5 min by pointing one of the optical fibres directly at the cells, and the other two were kept as control. The cells were allowed to grow under ideal conditions in an incubator at 37 °C and in a 5% CO_2 atmosphere. After four days the irradiated cells did not show any sign of difference to the control cells, which had not been irradiated. The total number of cells per dish increased to $(4.1 \pm 0.2) \times 10^5$ (control) and $(4.2 \pm 0.3) \times 10^5$ (irradiated) over the period of four days. This is the strongest test because it monitors whether the cells are still capable of dividing normally. In all the experiments the tests proved that the cells survive the conditions in an optical stretcher without any detectable damage. Likewise, the RBCs, which are particularly vulnerable due to their high content of highly absorbing haemoglobin, did not show any changes when trapped.

Another substantial question for the applicability of the optical stretcher to measure cell elasticities is whether cells maintain a cytoskeleton at all when they are trypsinized and in suspension. It has been indicated that cells dissolve their actin cytoskeleton when they are not in contact with each other or with a surface. Rhodamine–phalloidin staining clearly shows that these cells maintain an extensive actin network throughout the whole cell volume (see figure 5). In particular, the actin cortex can be seen at the rim of the cell. The only feature of the cytoskeleton that is not present are stress fibres. Considering the high Young's moduli for PC12 cells in suspension the fibres should play only a minor role in the elasticity of cells. The measured values are comparable to elasticity values reported for activated adhered platelets measured by atomic force microscopy [27].

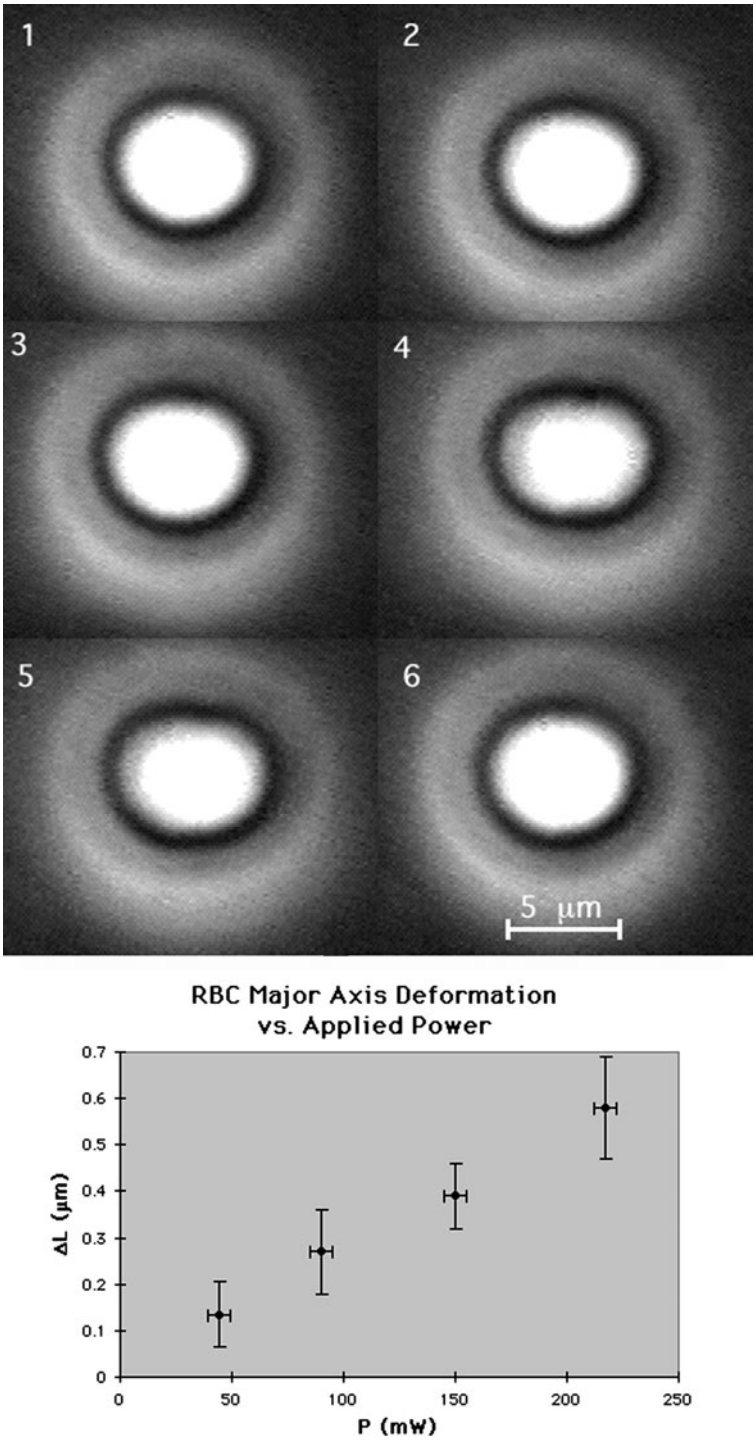

Figure 6. Sequence showing the stretching of an osmotically swollen RBC (upper panel). The time steps are 0.5 s. In steps 1–5 the power was increased from 5 to about 200 mW. In step 6 the stress on the cell was decreased again to show the reversibility of the deformation. Elongation ΔL of an RBC as function of the applied laser power P (lower panel).

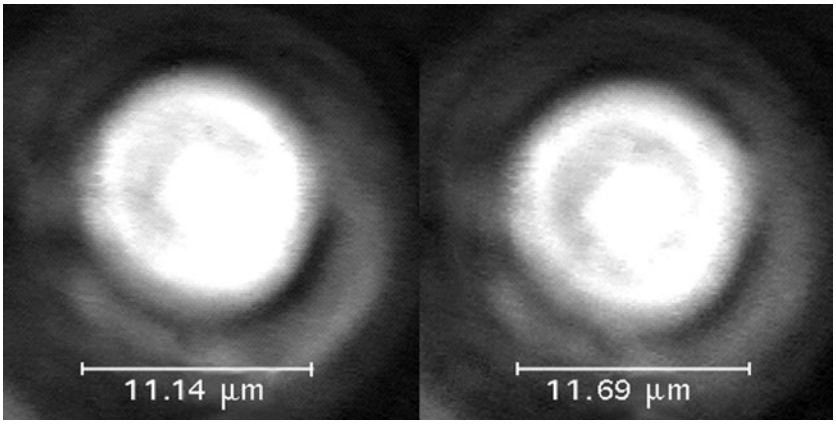

Figure 7. The stretching of a PC12 cell.

4. Results

As expected for a two-beam trap from previous studies on glass and latex beads [38, 41], cells were stably trapped with the optical stretcher at light powers of 2–10 mW. After trapping a cell the power was increased to its maximum values of 300 mW for RBCs and 500 mW for PC12 cells on a timescale of seconds. Due to the increasing stress the trapped cell was stretched as expected from our calculations.

Figure 6 shows a typical time sequence of the stretching of an RBC. The clearly visible deformation increases linearly with applied laser power. The peak stress applied to the cell was $\sigma = 1.57 \pm 0.03$ Pa, and the elongation along the major axis was from 6.08 ± 0.02 to 6.54 ± 0.02 μm. This is a relative deformation of $7.6 \pm 0.6\%$. The average deformation along the laser axis measured for ten RBCs was $7.5 \pm 0.3\%$ and, using equation (10), the homogeneous Young's modulus was $E = 11.0 \pm 0.5$ Pa. This value does not reflect the strength of the two-dimensional cytoskeleton of RBCs, which is much stronger. A more detailed analysis yields a cortical Young's modulus of $(3.9 \pm 1.4) \times 10^{-5}$ Pa [25]. These experiments illustrated that biological material can be stretched between two laser beams; it had still to be proven that forces can be generated that are sufficient to stretch eukaryotic cells.

In contrast to RBCs, PC12 cells have an extensive three-dimensional cytoskeleton and are much harder to deform (figure 7). The deformation is not as obvious as for RBCs (figure 6). The comparing of the horizontal width of the cell in the two pictures by image processing, however, reveals an elongation from 11.14 ± 0.02 to 11.69 ± 0.02 μm. The average deformation of PC12 cells along the laser axis was $4.2 \pm 0.2\%$ at a peak stress on the cell of $\sigma = 40 \pm 1$ Pa. With equation (10), the homogeneous Young's modulus is calculated to be $E = 500 \pm 25$ Pa. PC12 cells are thus 40–50 times stiffer than osmotically swollen RBCs.

To ensure that the deformation is real the following artifacts have been considered: since cells are not perfectly spherical the increase of the stress could cause the cell to rotate, which could lead to an increase of the measured diameter in the horizontal direction. This has been avoided by optical inspection. Another possibility is that the trapped cell is slightly away from the beam axis. When the intensity is increased, and the cell is pulled back towards the axis, the main cross-section moves out of the focal plane and the cell appears to be bigger. This can be ruled out because it would lead to an identical absolute increase in the horizontal and the vertical direction, which has not been observed.

5. Discussion

This work proves the feasibility of a nondestructive, optical tool for the quantitative deformation of cells—the optical stretcher. The radiation pressure of two counter-propagating laser beams of a cw Ti–sapphire laser at 780 nm is sufficient to deform a cell, which does not show any sign of detectable damage and maintains its normal cytoskeleton. Surprisingly, the cell is not squeezed but rather stretched out along the optical axis. This effect can be used to distinguish between different cells as demonstrated for RBCs and PC12 cells. These findings show that the optical stretcher is a tool that can distinguish between different cells by detecting phenomenological differences in their elasticities. In the same way it can be used for quantitative research on the cytoskeleton.

Changes in the cytoskeleton are often used to diagnose certain diseases such as cancer. A better understanding of the basic cytoskeletal cell biology will contribute to the understanding of the pathology of these disorders and can impact their diagnosis and therapy. Existing methods of cancer detection [43] rely on markers and/or optical inspection. Using measurements of cytoskeletal elasticity as an indicator for malignancy could be a novel approach in oncology. By using a microfluidic flow chamber, the optical stretcher could advance to a diagnostic tool in clinical laboratories. A flow chamber allows the handling of large numbers of cells and thus assures good statistics. This novel technique would require minimal tissue samples, which could be obtained by fine-needle aspiration using stereotactic, ultrasonographic or MRI guidance [44, 45].

Acknowledgments

This work was supported by NSF, NIH and Evacyte Corporation, Austin, TX.

References

[1] Ashkin A 1970 *Phys. Rev. Lett.* **24** 156–9
[2] Ashkin A 1978 *Phys. Rev. Lett.* **40** 729–32
[3] Ashkin A 1980 *Science* **210** 1081–8
[4] Svoboda K and Block S M 1994 *Annu. Rev. Biophys. Struct.* **23** 147–285
[5] Chu S 1991 *Science* **253** 861–6
[6] Cohen-Tannoudji C and Phillips W D 1990 *Phys. Today* October 33
[7] Phillips W D and Metcalf H J 1978 *Sci. Am.* March 50–6
[8] Ashkin A, Dziedzic J M, Bjorkholm J E and Chu S 1986 *Opt. Lett.* **11** 288–90
[9] Ashkin A 1992 *Biophys. J.* **61** 569–82
[10] Gussgard R, Lindmo T and Brevik I 1992 *J. Opt. Soc. Am.* B **9** 1922–30
[11] Kuo S C and Sheetz M P 1992 *Trends Cell Biol.* **2** 116–8
[12] Wright W H, Sonek G J and Berns M W 1993 *Appl. Phys. Lett.* **63** 715–7
[13] Visscher K and Brakenhoff G J 1992 *Optik* **89** 174–80
[14] Ashkin A and Dziedzic J M 1987 *Science* **235** 1517–20
[15] Ashkin A, Dziedzic J M and Yamane T 1987 *Nature* **330** 769–71
[16] Shepherd G M G, Corey D P and Block S M 1990 *Proc. Natl Acad. Sci. USA* **87** 8627–31
[17] Block S M, Goldstein L S B and Schnapp B J 1990 *Nature* **348** 348–52
[18] Kuo S C and Sheetz M P 1993 *Science* **260** 232–4
[19] Svoboda K, Schmidt C F, Schnapp B J and Block S M 1993 *Nature* **365** 721–7
[20] Simmons R M, Finer J T, Warrick H M, Kralik B, Chu S and Spudich J A 1993 *The Mechanism of Myofilament Sliding in Muscle Contraction* ed H Sugi and G H Pollack (New York: Plenum) pp 331–6
[21] Colon J M *et al* 1992 *Fertil. Steril.* **57** 695–8
[22] Tadir Y, Wright W H, Vafa O, Ord T, Asch R H and Berns W M 1990 *Fertil. Steril.* **53** 944–7
[23] Mehta A D, Rief M, Spudich J A, Smith D A and Simmons R M 1999 *Science* **283** 1689–95
[24] McKintosh F C, Käs J and Janmey P A 1995 *Phys. Rev. Lett.* **75** 4425

[25] Guck J, Ananthakrishnan R, Moon T J, Cunningham C C and Käs J 2000 *Phys. Rev. Lett.* **84** 5451–5
[26] Guck J, Ananthakrishnan R, Mahmood H, Moon T J, Cunningham C C and Käs J 2001 *Biophys. J.* **84** 767–84
[27] Radmacher M, Fritz M, Kacher C M, Cleveland J P and Hansma P K 1996 *Biophys. J.* **70** 556–67
[28] Felder S and Elson E L 1990 *J. Cell Biol.* **111** 2513–26
[29] Thoumine O and Ott A 1997 *J. Cell Sci.* **110** 2109–16
[30] Dailey B, Elson E L and Zahalak G I 1984 *Biophys. J.* **45** 661–82
[31] Discher D E, Mohandas N and Evans E A 1994 *Science* **266** 1032–5
[32] Wang N, Butler J P and Ingberg D E 1993 *Science* **260** 1124–7
[33] Elson E L 1988 *Annu. Rev. Biophys. Chem.* **17** 397–430
[34] Eichinger L, Koppel B, Noegel A A, Schleicher M, Schliwa M, Weijer K, Wittke W and Janmey P A 1996 *Biophys. J.* **70** 1054–60
[35] Roosen G and Imbert C 1976 *Phys. Lett.* A **59** 6–9
[36] Jackson J D 1975 *Classical Electrodynamics* (New York: Wiley)
[37] Ashkin A and Dziedzic J M 1973 *Phys. Rev. Lett.* **30** 139–42
[38] Constable A, Kim J, Mervis J, Zarinetchi F and Prentiss M 1993 *Opt. Lett.* **18** 1867–9
[39] Kats A V and Kantorovich V M 1969 *JETP Lett.* **9** 112–4
[40] Lure A I 1964 *Three-Dimensional Problems of the Theory of Elasticity* (New York: Interscience)
[41] Roosen G 1977 *Opt. Commun.* **21** 189–95
[42] Alberts B, Bray D, Lewis J, Raff M, Roberts K and Watson J D 1994 *Molecular Biology of the Cell* (New York: Garland)
[43] Sidransky D 1996 *Sci. Am.* September 104–9
[44] Fajardo L L and DeAngelis G A 1997 *Surg. Oncol. Clin. N. Am.* **6**
[45] Dunphy C and Ramos R 1997 *Diagn. Cytopathol.* **16** 200–6